Measuring plasma turbulence using low coherence microwave radiation

D. R. Smith[a)]
Department of Engineering Physics, University of Wisconsin-Madison, Madison, Wisconsin 53706, USA

(Received 20 December 2011; accepted 13 February 2012; published online 24 February 2012)

Low coherence backscattering (LCBS) is a proposed diagnostic technique for measuring plasma turbulence and fluctuations. LCBS is an adaptation of optical coherence tomography, a biomedical imaging technique. Calculations and simulations show LCBS measurements can achieve centimeter-scale spatial resolution using low coherence microwave radiation. LCBS measurements exhibit several advantages over standard plasma turbulence measurement techniques including immunity to spurious reflections and measurement access in hollow density profiles. Also, LCBS is scalable for 1-D profile measurements and 2-D turbulence imaging. © *2012 American Institute of Physics*. [http://dx.doi.org/10.1063/1.3690922]

Standard plasma turbulence diagnostics such as interferometry, reflectometry, and collective scattering employ coherent microwave sources and detectors.[1,2] This letter describes low coherence backscattering (LCBS), a plasma turbulence measurement technique using low coherence microwave sources and broadband detectors. Low coherence sources in the millimeter-wave or far infrared range with bandwidths $\Delta f \gtrsim 20$ GHz can measure plasma fluctuations with centimeter-scale spatial resolution. Among the advantages of LCBS are immunity to spurious reflections and measurement access in hollow density profiles. Also, the LCBS technique is expandable for 1-D profile measurements and 2-D imaging.

LCBS is adapted from optical coherence tomography (OCT), a biomedical imaging technique that performs depth scans in tissue using low coherence visible and near-infrared light sources.[3–5] OCT instruments conceptually resemble a Michelson interferometer and achieve 5–30 μm axial (depth) resolution at depths of 1–10 mm for tissue and cellular imaging. OCT measurements typically employ broadband superluminescent diodes with $\lambda_0 \approx 700 - 1500$ nm, $\Delta\lambda \approx 10 - 70$ nm, and $P \approx 5 - 50$ mW. The $1/e$ correlation length of a broadband source is

$$\Delta x = \frac{2\ln 2}{\pi}\frac{\lambda^2}{\Delta\lambda} \approx \frac{c}{2\Delta f}, \tag{1}$$

where λ is the center wavelength, $\Delta\lambda$ is the $1/e$ spectral width, Δf is the $1/e$ frequency bandwidth, and c is the speed of light.[5]

Broadband microwave or far infrared sources can achieve the centimeter-scale resolution needed for LCBS measurements of plasma turbulence. As shown in Figure 1, a microwave source with a 20 GHz bandwidth exhibits a 1.3 cm correlation length. An LCBS instrument, like OCT instruments, resemble a Michelson interferometer as shown in Figure 2. First, a beam splitter splits the source signal into a probe beam and reference signal. The plasma generates backscattered light[6] along the entire probe beam via collective Thomson scattering.[1,7,8] Next, the beam splitter combines the backscattered light and reference signal for detection. The reference signal travels a fixed path length. Backscattered light that travels a path length within a correlation length of the reference signal path length is coherent with the reference signal, and other backscattered light is incoherent. The detector is preferentially sensitive to backscattered light coherent with the reference signal, so the reference signal path length sets the measurement location along the probe beam. Immunity to probe beam spurious reflections is a corollary of the path length selectivity. A single reference signal and path length provide a single-point measurement, but multiple reference signals with different path lengths can measure a 1-D fluctuation profile. Similarly, a linear array of probe beams with multiple reference signals can provide 2-D fluctuation imaging.

LCBS measurements overcome several obstacles that limit standard plasma turbulence diagnostics. For instance, interferometry measurements are line-averaged, but LCBS measurements are localized along the probe beam. Probe beam spurious reflections compromise conventional scattering measurements, but LCBS measurements are immune to spurious reflections due to finite correlation length of the probe beam. Reflectometry measurements require complex wavefront modeling at the plasma cut-off layer, but LCBS measurements avoid wavefront and cut-off layer complications. Finally, hollow density profiles are inaccessible to reflectometry measurements, but not LCBS measurements.

The remainder of this letter contains a derivation of LCBS measurement principles and calculations that illustrate LCBS measurement capabilities.

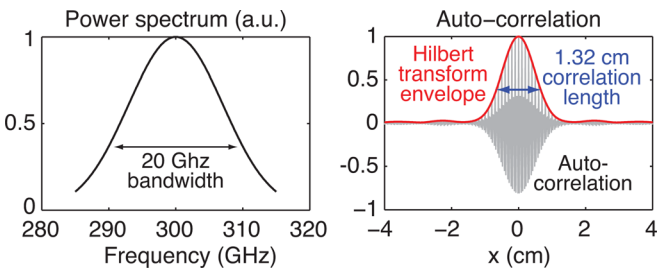

FIG. 1. (Color online) Power spectrum and spatial auto-correlation function for low coherence radiation with $\Delta f = 20$ GHz

[a)]Electronic mail: drsmith@engr.wisc.edu.

 © 2012 American Institute of Physics

Downloaded 25 Feb 2013 to 198.125.232.58. Redistribution subject to AIP license or copyright; see http://apl.aip.org/about/rights_and_permissions

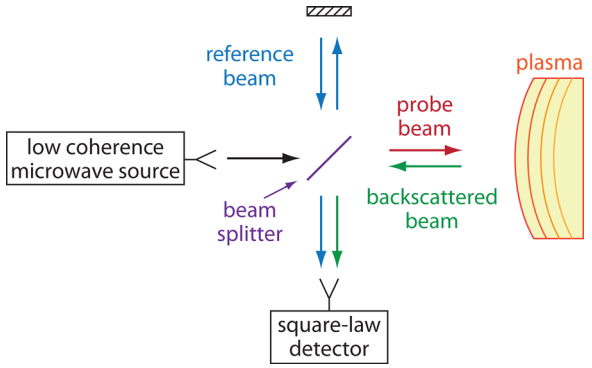

FIG. 2. (Color online) Schematic of a low coherence backscattering system.

LCBS measurements are collective Thomson scattering[1,7,8] from broadband radiation in a backscattering geometry.[6] The plasma generates backscattered light along the entire probe beam in response to the incident broadband radiation. Only backscattered light with a path length equal to the reference beam path length is coherent with the reference beam. The square-law detector receives backscattered light from the entire probe beam, but the detector is selectively sensitive to backscattered light coherent with the reference beam. As will be shown, the detector output provides a localized density measurement with a location set by the reference signal path length.

Consider a low coherence probe beam with electric field $E(x,t) = \int \tilde{E}(\omega) e^{i(kx-\omega t)} d\omega/2\pi$ where $\tilde{E}(\omega)$ is the complex-valued amplitude spectrum and $k = \omega/c$ is the vacuum dispersion. In the following derivation, assume $\omega \gg \omega_p$, where ω_p is the plasma frequency, so $k \approx \omega/c$ remains valid for propagation in plasma. Assume the detector and beamsplitter are located at $x = 0$ and the reference mirror is located a distance L from the beamsplitter. The reference signal arriving at the detector is

$$E_r(L,t) = E(2L,t) = \int \tilde{E}(\omega) e^{i\omega(2L/c)} e^{-i\omega t} \frac{d\omega}{2\pi}, \tag{2}$$

$$E_r(L,\omega) = \tilde{E}(\omega) e^{i\omega(2L/c)}. \tag{3}$$

The plasma response to the probe beam generates the backscattered signal

$$E_{bs}(x,t) = \int_{x_{min}}^{x_{max}} \frac{r_e A}{|x-x'|} n_e(x',t') E(x',t') dx', \tag{4}$$

where r_e is the classical electron radius, A is the probe beam cross-section area, n_e is the plasma electron density, $t' \equiv t - |x-x'|/c$ is the retarded time, and x_{min} and x_{max} are the plasma boundaries. Plasma density fluctuations are slow compared to probe beam oscillations and transit times, so let $n_e(x',\tau)$ denote density profiles stationary on the timescales of t and t'. The backscattered signal arriving at the detector is

$$E_b(t) = E_{bs}(0,t) \tag{5}$$

$$= \int_{x_{min}}^{x_{max}} \frac{r_e A}{x'} n_e(x',\tau) E(0, t - 2x'/c) dx' \tag{6}$$

$$= \int_{x_{min}}^{x_{max}} \frac{r_e A}{x'} n_e(x',\tau) dx' \ldots$$

$$\times \int \tilde{E}(\omega) e^{i\omega(2x'/c)} e^{-i\omega t} \frac{d\omega}{2\pi}, \tag{7}$$

$$E_b(\omega) = \tilde{E}(\omega) \int_{x_{min}}^{x_{max}} \frac{r_e A}{x'} n_e(x',\tau) e^{i\omega(2x'/c)} dx'. \tag{8}$$

The reference and backscattered signals combine at the detector. Consider a square-law detector with response time, T, faster then plasma fluctuation timescales. The net signal at the detector is $E_r(t) + E_b(t)$, so the low frequency detector output is

$$V(L,\bar{t}) = \langle |E_r(L,t) + E_b(t)|^2 \rangle_T \tag{9}$$

$$= \langle |E_r|^2 + |E_b|^2 + 2E_r^*(L,t) E_b(t) \rangle_T, \tag{10}$$

$$\tilde{V}(L,\bar{t}) = 2\langle E_r^*(L,t) E_b(t) \rangle_T \tag{11}$$

$$= \frac{2}{T} \int_{T/2}^{T/2} E_r^*(L,t) E_b(t) dt \tag{12}$$

$$= \frac{2}{T} \int E_r^*(L,\omega) E_b(\omega) \frac{d\omega}{2\pi}, \tag{13}$$

where $\bar{t}$ is the average time of the detector response period. $\langle |E_r|^2 \rangle_T$ and $\langle |E_b|^2 \rangle_T$ are dc signals, but the time-dependent signal $\tilde{V}(L,\bar{t})$ contains information about plasma fluctuations. Substituting Eqs. (3) and (8) into Eq. (13) gives

$$\tilde{V}(L,\bar{t}) = \frac{2}{T} \int_{x_{min}}^{x_{max}} \frac{r_e A}{x'} n_e(x',\tau) dx' \ldots$$

$$\times \int e^{i\omega(2/c)(x'-L)} |\tilde{E}(\omega)|^2 \frac{d\omega}{2\pi} \tag{14}$$

$$= \frac{2P_0}{T} \int_{x_{min}}^{x_{max}} \frac{r_e A}{x'} n_e(x',\tau) dx' \ldots$$

$$\times \int e^{i\omega(2/c)(x'-L)} e^{-(\omega-\omega_0)^2/\Delta\omega^2} \frac{d\omega}{2\pi}, \tag{15}$$

where $|\tilde{E}(\omega)|^2 = P_0 e^{-(\omega-\omega_0)^2/\Delta\omega^2}$ is the probe beam power spectrum. Evaluating the second integral in Eq. (15) gives

$$\int e^{i\omega(2/c)(x'-L)} e^{-(\omega-\omega_0)^2/\Delta\omega^2} \frac{d\omega}{2\pi}$$

$$= \frac{\Delta\omega}{2\sqrt{\pi}} e^{i\omega_0(2/c)(x'-L)} e^{-(x'-L)^2\Delta\omega^2/c^2}. \tag{16}$$

Now Eq. (15) is

$$\tilde{V}(L,\bar{t}) = \frac{P_0 \Delta\omega r_e A}{T\sqrt{\pi}} \int_{x_{min}}^{x_{max}} \frac{n_e(x',\tau)}{x'} \ldots$$

$$\times e^{i\omega_0(2/c)(x'-L)} e^{-(x'-L)^2\Delta\omega^2/c^2} dx'. \tag{17}$$

Equation (17) can be written

$$\tilde{V}(\bar{t}) = \frac{P_0 c r_e A}{TL} \mathcal{N}_e(L,\tau), \tag{18}$$

where

Downloaded 25 Feb 2013 to 198.125.232.58. Redistribution subject to AIP license or copyright; see http://apl.aip.org/about/rights_and_permissions

$$\mathcal{N}_e(L,\tau) \equiv \frac{L\Delta\omega}{c\sqrt{\pi}} \int_{x_{min}}^{x_{max}} \frac{n_e(x',\tau)}{x'} e^{i\omega_0(2/c)(x'-L)} \cdots \times e^{-(x'-L)^2\Delta\omega^2/c^2} dx' \quad (19)$$

is a density-like quantity. Note that the integral in Eq. (19) is preferentially sensitive to the region $x' \approx L \pm c/\Delta\omega$ and

$$n_e(L,\tau) = \lim_{\Delta\omega\to\infty} \mathcal{N}_e(L,\tau). \quad (20)$$

Therefore, the combined reference and backscattered signals (Eqs. (3) and (8)) averaged over the response time of a square-law detector (Eqs. (9) and (11)) give a localized density measurement at a location set by the reference beam path length (Eq. (18)).

The single-point measurement described above can be generalized to 1-D and 2-D measurements. A 1-D profile measurement can be obtained by splitting the reference and backscattered beams into multiple beams and imposing different path lengths on the reference beams. When reference and backscattered beams recombine at detectors, the output signals are preferentially sensitive to density fluctuations at locations set by the path lengths of the multiple reference beams. In this way, a single probe beam can provide a 1-D profile measurement. Similarly, an array of probe beams, each with multiple reference beam path lengths, enables 2-D fluctuation imaging.

Simulated measurements can demonstrate the capabilities of the LCBS technique. Figures 3(a) and 3(b) show low coherence probe beams with bandwidths $\Delta f = 14$ GHz and 40 GHz. The spatial resolutions are 1.9 cm and 0.7 cm, respectively. The simulated density profile in Figures 3(c) and 3(d) includes random fluctuations. Reference signals are obtained from Eq. (2), and backscattered signals are obtained from Eq. (7). Figures 3(c) and 3(d) show the simulated density profile and LCBS reconstructions of the density profile. The LCBS measurements qualitatively capture profile variations, including hollow density features, down to the measurement spatial resolutions. As expected, the broader-band measurement ($\Delta f = 40$ GHz) captures more profile features and exhibits a smaller root-mean-square (RMS) error relative to the specified density profile.

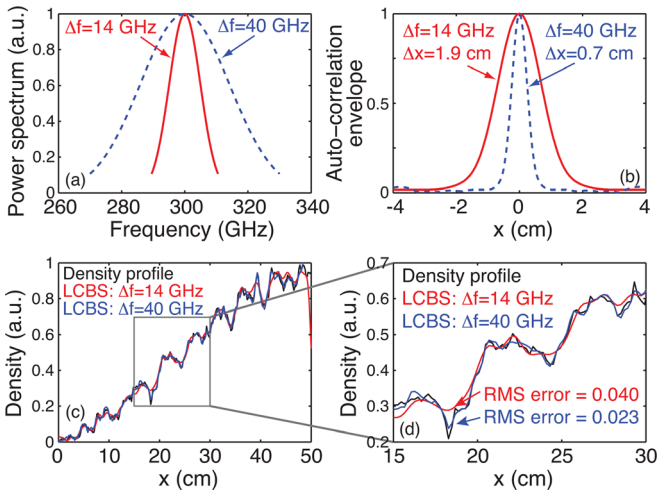

FIG. 3. (Color online) (a) Power spectra and (b) auto-correlation envelopes for low coherence probe beams. (c) and (d) show a simulated density profile and LCBS reconstructions ($\Delta f = 14$ GHz and $\Delta f = 40$ GHz).

LCBS is a proposed technique for measuring plasma turbulence and fluctuations. The technique is an adaptation of optical coherence tomography, a biomedical imaging technique. LCBS measurements exploit the finite correlation length of low coherence microwave radiation ($\Delta f \gtrsim 20$ GHz) to achieve centimeter-scale spatial localization (Figure 3). The time-dependent signal from a square-law detector provides a localized density fluctuation measurement (Eq. (18)). The diagnostic advantages of LCBS include immunity to spurious reflections, measurement access in hollow density profiles, and scalability for 1-D profile measurements and 2-D turbulence imaging.

This work was supported by U.S. Department of Energy Grant No. DE-SC0001288.

[1]N. C. Luhmann, Jr. and W. A. Peebles, Rev. Sci. Instrum. **55**, 279 (1984).
[2]R. Nazikian, G. J. Kramer, and E. Valeo, Phys. Plasmas **8**, 1840 (2001).
[3]P. H. Tomlins and R. K. Wang, J. Phys. D **38**, 2519 (2005).
[4]J. G. Fujimoto, Nat. Biotechnol. **21**, 1361 (2003).
[5]A. F. Fercher, W. Drexler, C. K. Hitzenberger, and T. Lasser, Rep. Prog. Phys. **66**, 239 (2003).
[6]T. L. Rhodes, W. A. Peebles, X. Nguyen, M. A. V. Zeeland, J. S. deGrassie, E. J. Doyle, G. Wang, and L. Zeng, Rev. Sci. Instrum. **77**, 10E922 (2006).
[7]E. Mazzucato, Phys. Rev. Lett. **36**, 792 (1976).
[8]R. E. Slusher and C. M. Surko, Phys. Fluids **23**, 472 (1980).

Downloaded 25 Feb 2013 to 198.125.232.58. Redistribution subject to AIP license or copyright; see http://apl.aip.org/about/rights_and_permissions